ELSEVIER

Contents lists available at ScienceDirect

Quaternary Science Reviews

journal homepage: www.elsevier.com/locate/quascirev



Variability in effective moisture inferred from inclusion fluid δ^{18} O and δ^{2} H values in a central Sierra Nevada stalagmite (CA)



Barbara E. Wortham a,* , Isabel P. Montañez a , Peter K. Swart b , Hubert Vonhof c , Clay Tabor d

- ^a Earth and Planetary Sciences Department and John Muir Institute of the Environment, University of California, Davis, CA, USA
- ^b Rosenstiel School of Marine and Atmospheric Sciences, University of Miami, FL, USA
- ^c Climate Geochemistry Department, Max Planck Institute of Chemistry, Mainz, Germany
- ^d Department of Geosciences, University of Connecticut, Storrs, Connecticut, USA

ARTICLE INFO

Article history: Received 20 January 2022 Accepted 21 January 2022 Available online 3 February 2022

Handling Editor: Prof. C. Hillaire-Marcel

Keywords: Speleothem Stable isotopes Fluid inclusions Isotope enabled modeling

ABSTRACT

The oxygen isotopic composition of stalagmites is widely used to infer regional changes in terrestrial surface temperatures and precipitation dynamics. The stalagmite $\delta^{18}O$ values, however, record the influence of multiple environmental conditions (e.g., temperature, precipitation source and amount) as well as in-cave physicochemical processes and possible disequilibrium precipitation effects. The $\delta^{18}O$ and δ^2H values of fluids entombed in stalagmites as inclusions have the potential to be robust proxies of paleo-precipitation $\delta^{18}O$ and δ^2H . Here we analyze the inclusion-fluid $\delta^{18}O$ and δ^2H values for a stalagmite from a central Sierra Nevada foothill cave, McLean's Cave, to reconstruct changes in effective moisture (precipitation — evaporation) in the region over the last deglaciation (20–13 ka). The results demonstrate high variability in inclusion-fluid $\delta^{18}O$ and δ^2H values and further suggest that the $\delta^{18}O$ and δ^2H values have several intervals driven by disequilibrium dis oxygen isotopic fractionation. These findings demonstrate that effective moisture was likely lower during past warm periods in comparison to some colder periods, consistent with other stalagmite calcite-based paleoclimate records from the southwestern United States.

© 2022 The Authors. Published by Elsevier Ltd. This is an open access article under the CC BY license (http://creativecommons.org/licenses/by/4.0/).

1. Introduction

Variability in the amount of precipitation over the last deglaciation (20–11 ka) in the southwestern U.S. ('Southwest') has long been linked to changing Northern Hemisphere temperature and continental ice volume (Oster et al., 2009, 2015; Allen and Anderson, 2000; Owen et al., 2003; Quade and Broecker, 2009; McGee et al., 2012; Street et al., 2012; Broecker and Putnam, 2013; Munroe and Laabs, 2013; Oster et al., 2015). During the last deglaciation, stalagmite proxy records from California, and other regions of the Southwest, suggest increased and/or seasonally shifted effective moisture (precipitation — evaporation) during past stadials in comparison to interstadial periods (Asmerom et al., 2010, 2017; Wagner et al., 2010; Lachniet et al., 2014, 2016; Oster et al., 2009, 2015). This finding corroborates precipitation records for this region developed using independent terrestrial proxies

response, remains limited. This incomplete understanding is in part due to the multiple environmental conditions and physicochemical processes, such as temperature (via fluid-calcite oxygen isotope fractionation) and precipitation amount and source, as well as incave processes that influence calcite δ^{18} O values (δ^{18} O_{cc}) (Hendy, 1971; McDermott, 2004; Lachniet, 2009). For example, studies of California (CA) stalagmites differ in their interpretations of the

terization (Hudson et al., 2019; Oster et al., 2020).

(Kirby et al., 2013; McGee et al., 2018; Feakins et al., 2019; Santi et al., 2020). This hypothesized hydroclimate regime of wetter

stadials and drier interstadials, however, does not conform with all

paleoclimate reconstructions for the last deglaciation (Bacon et al.,

2006; Benson et al., 2003) and may be an oversimplistic charac-

ka, our understanding of the sensitivity of the precipitation

response in this region to millennial- and centennial-scale climate change, and of the underlying climate dynamics governing the

primary driver of temporal changes in $\delta^{18}O_{cc}$ with variability in temperature, precipitation amount or source invoked (Oster et al.,

Despite a rich proxy archive for the Southwest over the past ~20

^{*} Corresponding author.

E-mail address: babswortham@berkeley.edu (B.E. Wortham).

2009, 2014, 2015, 2020; De Wet et al., 2021). Thus, a proxy independent of $\delta^{18}O_{cc}$ is needed to deconvolve the combined influences of temperature, precipitation parameters (e.g., source, evolution of the $\delta^{18}O$ composition of vapor ($\delta^{18}O_v$) and precipitation ($\delta^{18}O_p$) along the storm track, rainout amount), and in-cave processes (i.e., rapid CO_2 degassing, evaporation).

Here we present a time series of $\delta^{18}O$ and δ^2H values of fluids entombed as inclusions (herein referred to as $\delta^{18}O_{fi}$ and δ^2H_{fi}) from a central Sierran stalagmite (ML-1 from McLean's Cave) that provides new insight into how precipitation varied in this region with changing mean climate between 19 and 13 ka. Furthermore, we evaluate calculated variables: d-excess, $\Delta\delta^{18}O$ ($\delta^{18}O_{cc}$ - $\delta^{18}O_{fi}$), and temperature. We use these to determine drivers of variability in the $\delta^{18}O_{fi}$ and δ^2H_{fi} record. Finally, we compare the time-series from this record to previously developed calcite proxy records ($\delta^{18}O_{cc}$, $\delta^{13}C_{cc}$, and Sr/Ca) from stalagmite ML-1 and to $\delta^{18}O_{cc}$ records from across the Southwest.

2. Background

The $\delta^{18}O_{fi}$ and δ^2H_{fi} values of stalagmites have the potential to deconvolve the influences on measured $\delta^{18}O_{cc}$ values (nomenclature described in Table 1). Previous studies have documented the potential of $\delta^{18}O_{fi}$ and $\delta^{2}H_{fi}$ values as reliable proxies of the local paleo-precipitation ($\delta^{18}O_p$ and δ^2H_p) when a clear relationship between the isotopic compositions of drip water and local precipitation can be established (Affolter et al., 2015; Dassie et al., 2018; Arienzo et al., 2019). In turn, $\delta^{18}O_{fi}$ and $\delta^{2}H_{fi}$ values have been used to infer variability in moisture-source (Rogerson et al., 2019), precipitation amount (Millo et al., 2017), or mean-annual-temperature (McGarry et al., 2004; Griffiths et al., 2010; Ayalon et al., 2013; Meckler et al., 2015; Arienzo et al., 2015; Affolter et al., 2019). Environmental monitoring in a Sierran foothill cave (Black Chasm), proximal (~80 km) to McLean's Cave, establishes a relationship between drip-water δ^{18} O and δ^{2} H values and precipitation source (Oster et al., 2012). Therefore, we hypothesize that the measured $\delta^{18}O_{fi}$ and $\delta^{2}H_{fi}$ values from the ML-1 stalagmite have the potential to preserve variability in $\delta^{18}O_p$ and δ^2H_p values in ideal cave conditions.

An additional benefit of measuring $\delta^{18}O_{fi}$ and δ^2H_{fi} values, that is rarely applied, is determining to what extent disequilibrium fractionation is influencing a stalagmite proxy time series and in turn, to reconstruct the temporal variability in equilibrium vs. disequilibrium effects. Disequilibrium fractionation of stable isotopes in cave calcite deposits occurs because of low humidity and/or rapid CO₂ degassing (Mickler et al., 2004, 2006; Dreybrodt and Deininger, 2014). These processes are driven by climate variability, as relative humidity in the cave is frequently lower with lower effective moisture (Forbes, 1998; Oster et al., 2012), and CO₂ degassing is linked to the CO₂ composition of the cave, which in turn is related to vegetation variability and surface air temperature (Banner et al., 2007; Wong and Banner, 2010; Wong et al., 2011). Lower effective moisture in terrestrial settings leads to greater evaporation. Evaporation from terrestrial water bodies, such as lakes, soil water, rivers, and snowpack lead to a greater difference between ²H and ¹H in these water bodies relative to the difference between ¹⁸O and ¹⁶O in the same bodies of water. The difference, caused by evaporation, defines a linear relationship between the $\delta^{18}\text{O}$ and $\delta^2\text{H}$ values that is shifted from the local meteoric water line and that has a lower slope (Rozanski et al., 1993; Lachniet, 2009). The effect is relevant for all places from which water can be evaporated, such as the thin film on a stalagmite surface. This effect is noted in the calculated variable *d*-excess, which decreases through evaporation in terrestrial settings (Rozanski et al., 1993; Clark and Fritz, 1997; Anderson et al., 2016) and has been noted in $\delta^{18}O_{fi}$ and $\delta^{2}H_{fi}$

(Warken et al., 2021).

Alternatively, rapid CO₂ degassing from drip water and thin films on stalagmites, driven by surface temperatures (via cave ventilation) and vegetation and its impact on stable isotope values has been evaluated in cave monitoring studies (e.g., Mickler et al., 2004, 2006). In many modern cave studies rapid CO₂ degassing leads to an increased difference between the δ^{18} O values of the drip water and the dissolved inorganic carbon (DIC) pool within it, a change that is recorded in stalagmite calcite as an increase in $\Delta\delta^{18}O$ (Mickler et al., 2004, 2006; Dreybrodt and Deininger, 2014). In this case, observations of the stalagmite calcite and water would show larger difference between water $\delta^{18}O$ and calcite $\delta^{18}O$ values (or $\Delta \delta^{\bar{1}8}$ O; Table 1). Alternatively, kinematic models of stable isotopic fractionation in supersaturated fluid conditions can lead to changes in calcite crystal kink dynamics in the calcite structure that cause a decrease in $\Delta\delta^{18}$ O values. Kink dynamics are driven by variable water pH at a stalagmite surface (Watkins et al., 2014). Although seemingly in conflict, the two interpretations of $\Delta\delta^{18}O$ demonstrate that kinetic fractionation led to a $\Delta \delta^{18}$ O that is not expected based on equilibrium conditions. To better evaluate the mechanism of kinetic fractionation, it is crucial that all aspects of the $\delta^{18}O_{fi}$ and δ^2 H_{fi} values be analyzed including other calculated variables (dexcess and temperature) and the relationship of the $\delta^{18}O_{fi}$ and δ^2H_{fi} values to the local meteoric water line. Temperature is crucial and defining a range of reasonable temperatures for a cave setting in the modern is straightforward through cave monitoring. Extensive cave monitoring has been done in a nearby cave to ML-1. Black Chasm (~80 km away: Oster et al., 2012) and a range of modern cave temperatures is defined as 10-20 °C. Additionally, several temperature reconstructions based on geologic evidence and models demonstrate that the temperature of California warmed between 6 and 5 °C since the Last Glacial Maximum (e.g., Tierney et al., 2020). Thus, we hypothesize that 1. evaluating the $\delta^{18}O_{fi}$ and $\delta^{2}H_{fi}$ results in relation to the meteoric water lines, 2. calculating a $\Delta\delta^{18}$ O in theoretical equilibrium conditions and comparing this to calculated $\Delta\delta^{18}O$ based on measurements in stalagmite ML-1, and 3. calculating a *d*-excess and a temperature for each $\delta^{18}O_{fi}$ and $\delta^{2}H_{fi}$ result through time will highlight variability in equilibrium and kinetic fractionation within stalagmite ML-1.

3. Methods

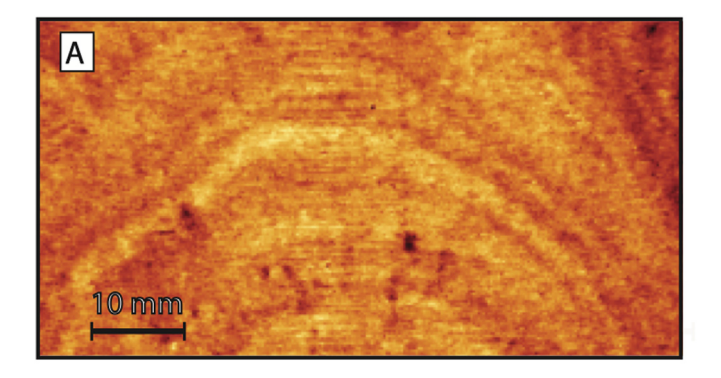
3.1. Fluid inclusion analysis

Stalagmite ML-1 was previously U—Th dated and analyzed for calcite-based geochemical and stable isotopic compositions (Santare, 2013; Oster et al., 2015). Sample ML-1 is 22.5 cm long (Supp. Fig. 1) and grew between 19.4 \pm 0.3 and 11.7 \pm 0.4 ka based on 10 U—Th dates. The age/depth model for ML-1 (Supp. Fig. 1) was re-evaluated in this study using CoPRA (Brietenbach et al., 2012) to incorporate Monte Carlo estimations of age uncertainty (2000 iterations by default). The age of the inclusion fluids in this study are 19.1 to 12.9 ka. Details on McLean's Cave and the calcite proxy time series can be found in Santare (2013), Oster et al. (2015), and Wortham et al. (2019).

Stalagmite intervals best suited for inclusion fluid analysis were identified by coupling neutron and X-ray computed tomography, an approach that has been documented to successfully identify intervals rich in fluid-vs. air-filled inclusions (Wortham et al., 2019). Sampling density through time is driven by the growth rate of the stalagmite and finding layers in the NCT and XCT scanning that were fluid-filled. Petrographic study and coupled XCT and NCT scanning reveal distribution and density of fluid-filled inclusions along the growth axis of the stalagmite. Along a growth band there is a consistent distribution of fluid-filled inclusions (Fig. 1A;

Wortham et al., 2019). Physically isolating a given growth band from mm-thick wafers of stalagmite (prepared from 2 by 1 inch thin-section billets) for inclusion fluid analysis is challenging due to the sub-mm spatial scale of bands. In this study, when a given wafer was split in half to be analyzed twice for $\delta^{18}O_{\rm fl}$ and $\delta^2H_{\rm fl}$ values (Fig. 1B), the two analyses are considered duplicates and not true replicates. The average of the two duplicates is presented in each plot and used for statistical analyses.

Fluid-rich regions in ML-1 (Fig. 1) were sampled as 200-500 mg chips (X:Y:Z dimensions of 0.25-0.50 cm: 1 cm: 0.25 cm) taken from wafers that were previously cut from thin-section billets. Analysis of the inclusion fluids in 31 chips (n = 41 analyses including duplicates) was performed on a speleothem crushing line connected to a Picarro L2130-i cavity ring-down spectroscope at the Rosenstiel School for Marine and Atmospheric Sciences (RSMAS), University of Miami, FL (Supp. Fig. 2). The crushing line consists entirely of stainless steel 1/8" external diameter tubing (SS-T2-S-6ME, Swagelok, Mulberry, FL, USA). The entire extraction line is heated with nickel-chromium resistance heating wire with fiberglass sleeving (NI80-015, FBGS-N-22, OMEGA Engineering, Stamford, CT, USA). Crushing of the sample occurs in a modified 3/ 8" Nupro vacuum valve (Swagelok SS-6BG; Arienzo et al., 2013) by manually spinning the handle of the valve to slowly crush the stalagmite sample to a powder. Heating of the crushing unit is accomplished by a 100 W cartridge heater inserted into a base plate on which the crusher valve rests. A continuous flow of N₂ is present through the line to the CRDS. The original version of the crushing line was presented in Arienzo et al. (2013). In this study, we



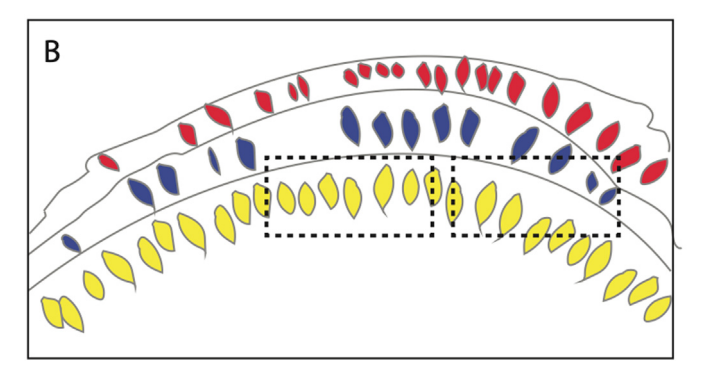


Fig. 1. Coupled NCT and XCT scan and schematic of fluid inclusion distribution in ML-1 growth bands. (A) Coupled CT image exhibits fluid-filled inclusion-rich bands (light yellow) alternating with bands of inclusion-poor bands (darker orange; modified from Wortham et al., 2019). Photo resolution is limited by the voxel size in the scans. (B) Schematic of the fluid inclusion distribution illustrates how adjacent duplicate samples (dashed boxes) required for analytical 'replicates' may sample variable proportions of discrete generations (indicated by colors) of included fluids. (For interpretation of the references to color in this figure legend, the reader is referred to the Web version of this article.)

modified this approach substantially as follows. The two main changes are:

- 1. **Analyses.** A quartz tube with platinum wire was connected to the crushing line (Supp. Fig. 2) and heated to 400 °C. The quartz tube was added to reduce interference in the CRDS created by the presence of organic molecules (Supp. Fig. 2) (cf. Dassie et al., 2018), which are known to deleteriously affect the δ^{18} O values by interfering at the wavelengths used. Although this approach produces a small amount of H₂O, its effect on the δ^{18} O of the H₂O samples is minimal (Zheng et al., 2018).
- 2. **Data reduction.** The H_2O released from the crushed sample or liquid injection was allowed to enter directly into the CRDS in a continuous flow, producing a sharp H_2O peak (Supp. Fig. 3) as the water released enters the system and then the signal dies away. No expansion volume was used. The $^{18}O/^{16}O$ ratio was determined by integrating the ^{18}O and ^{16}O peaks and the same was done for the $^{2}H/^{1}H$ ratio. The Picarro software analyzes the $\delta^{18}O$ and $\delta^{2}H$ values every 0.1 s. To determine a $\delta^{18}O$ and $\delta^{2}H$ value, the δ value was weighted by the amount of water (ppm) being measured in the same 0.1 s. An average was taken of the weighted stable isotope value. All analyses for which the water amount was >200 ppm was used in the weighted average.

A diagram depicting a typical analysis is presented in Supp. Fig. 4. To summarize, at the beginning of each day of analysis several liquid injections of an in-lab standard were analyzed until a stable signal was achieved. The water was injected through the water injection port (Swagelok SS-4-T), which allowed for 0.1–1.2 μL of standard waters to be injected (Arienzo et al., 2013). The first injections of the day were analyzed to ensure that the speleothem line was not leaking, that there was a stable flow of N₂, and that the line was evenly heated to 115 °C. Following this first test, a 'memory' test was performed by analyzing three injections of one in-lab standard followed by three injections of another in-lab standard of a different known value. The values were determined using the reduction procedure referred to in point (2). A curve was then fitted to the determined values from the memory test and was applied as a 'memory correction' to the rest of the analyses that day. Subsequently, for each stalagmite sample (and rock standard treated as an unknown) was bracketed by three measurements of an in-lab standard (0.5 μ L) before and after the stalagmite sample (Arienzo et al., 2013). A test was performed daily to determine whether the size of the liquid standard injection impacted the calculated stable isotope value, referred to as the 'size effect'. No size effects were detected throughout the period of analysis. The bracketed injections and the memory test for the day were used to correct the unknowns. Of note, the addition of the heated quartz tube was assessed as an effective change to reducing organic contamination by measuring the WICO standards, one of which (WICO-5) was spiked with methanol to mimic organic contamination (Western Regional Climate Center,). The measurement of WICO-5 yielded a value within uncertainty of the known value when measured using the methodology presented here. Additionally, the new reduction method used in this study improves the sensitivity of the method by an order of magnitude.

Uncertainty on each individual measurement is calculated by taking the average 1σ standard deviation of the liquid injection standards that bracketed each analysis. An average uncertainty for the method is calculated by taking the average 1σ uncertainty from the liquid standards and repeated analyses of modern flowstones (Supp. Fig. 4). Based on these analyses, the analytical precision (1σ) for the method presented here is 0.6% and 5.2% for $\delta^{18}O_{fi}$ and δ^2H_{fi} , respectively. In addition, a subset of stalagmite chips (duplicates of those run at RSMAS; n=9) were analyzed on a TC-EA IRMS

in the Stable Isotope Laboratory, Max Planck Institute for Chemistry (MPIC), Mainz, Germany (Vonhof et al., 2006; De Graaf et al., 2020) to determine the relative offset between CRDS and TC-EA IRMS methods (Supp. Table 2). The correction method for memory effect and to standards employed at MPIC is the same to that employed at RSMAS. Analytical precision (1σ) for the TC-EA IRMS at MPIC based on repeated measurements of standard waters and minerals is 0.5% and 5.0% for $\delta^{18} O_{fi}$ and $\delta^2 H_{fi}$, respectively. All duplicates were averaged together.

3.2. Data analysis

We follow the time-interval differentiation for the last deglaciation proposed by Oster et al. (2020): Late Glacial (LG, 19.3 to 18.0; n = 8 samples analyzed), Heinrich Stadial 1a (18.0–16.1 ka, n = 8), Heinrich Stadial 1b (16.1–14.6 ka; n = 8), the Older Dryas stadial (OD, 14.1 to 13.8 ka; n = 5), and the Bölling and Allerød interstadials (14.6-14.1 ka and 13.8 to 12.8 ka, respectively; n = 12). Two phases of Heinrich Stadial 1 have been previously denoted as the "Big Dry" and the subsequent "Big Wet" (Broecker et al., 2009). Recently, inconsistencies in effective moisture reconstructions for the Southwest have been documented suggesting that the two phases of HS-1 may not be regional (cf. Hudson et al., 2019); thus, we refer to the two phases of Heinrich Stadial 1 as HS1a and HS1b. Results for the warmer Bölling and the Allerød interstadials (<1 ky duration each) were combined given their brief duration and that these two warm intervals were punctuated by a brief cooling and refer to the combined intervals as the B/A (Bölling/Allerød).

To assess whether equilibrium oxygen isotope fractionation between drip water and calcite occurred during stalagmite ML-1 formation and to evaluate the potential influence of evaporation on inclusion fluid and stalagmite calcite isotopic compositions, we calculated three variables using the measured $\delta^{18}O_{fi}$ and $\delta^{2}H_{fi}$ and $\delta^{18}O_{cc}$ values and using the modern precipitation values from the region. The first, $\Delta \delta^{18}$ O, is the difference between measured δ^{18} O_{cc} (converted to VSMOW) and $\delta^{18}O_{fi}$ values (Table 1). Given the very different temporal resolutions of the $\delta^{18}O_{cc}$ and $\delta^{18}O_{fi}$ data sets for ML-1, the stalagmite $\delta^{18}O_{cc}$ values (n = 617; Santare, 2013; Oster et al., 2015) were bin-averaged to match the temporal resolution (100–200 yr) of the $\delta^{18}O_{fi}$ and δ^2H_{fi} analyses before calculating the $\Delta \delta^{18}$ O values for each δ^{18} O_{fi} datum. Predicted equilibrium $\Delta \delta^{18}$ O was estimated using the bin-averaged $\delta^{18}O_{cc}$ values for the ML-1 stalagmite and temperatures of 7.0, 10.0, and 12.3 °C based on cave monitoring at Black Chasm (~80 km away; Oster et al., 2012). These values were applied to the calcite-water oxygen isotope fractionation equations of Daeron et al. (2019) and Tremaine et al. (2011). The second variable, d-excess, was calculated for each inclusion data point to assess the potential influence of evaporation on inclusion-fluid isotopic compositions. We note here that the definition of d-excess used in this study is based on previous researchers working in cave and terrestrial environments and is therefore focused on the process of rainwater recycling driven by evaporation (e.g., Lachniet, 2009; Anderson et al., 2016). The dexcess, or deuterium excess, is the 'y-intercept' of the best-fit line through the $\delta^{18}O$ and $\delta^{2}H$ values distributed on a x- and y-plot. We calculate the d-excess using the following equation: dexcess = $\delta^2 H_{\rm fi}$ - (7.9 * $\delta^{18} O_{\rm fi}$) as defined by the Local Meteoric Water Line for the study area (Oster et al., 2012). The third calculated variable is temperature of precipitation for each pair of measured $\delta^{18}O_{fi}$ values and their corresponding binned $\delta^{18}O_{cc}$ value using the temperature fractionation equations of Tremaine et al. (2011) and Daeron et al. (2019).

Furthermore, we compare the measured $\delta^{18}O_{fi}$ values to precipitation $\delta^{18}O$ compositions obtained using the Community Earth System Model version 1.3 with isotopologue tracking for $\delta^{18}O$

(iCESM1.3) for time slices throughout the deglaciation at 21.0, 16.0 (with and without fresh water forcing), 15.0, 14.0, and 12.5 ka (Tabor et al., 2021). The boundary conditions and parameterization of iCESM1.3 is described in He et al. (2021) and Tabor et al. (2021). The climate and water isotopologues in iCESM1.3 were spun up using the fully coupled configuration of iCESM1.3 with a $1.9^{\circ} \times 2.5^{\circ}$ horizontal resolution atmosphere (Community Atmosphere Model 5: CAM5) and land (Community Land Model 4: CLM4) components. and nominal 1° horizontal resolution ocean (Parallel Ocean Program 2; POP2) and sea ice (Community Sea Ice Model 4; CICE4) components (He et al., 2021). To spin-up the land model (notably, soil temperatures and hydrology) at higher resolution, we first interpolated the results from the $1.9^{\circ} \times 2.5^{\circ}$ resolution simulations to the $0.9^{\circ} \times 1.25^{\circ}$ grid, then ran the CAM5/CLM4-only simulations for 50 years using an annual cycle of sea-surface conditions from the mean of the final 50 years of the fully coupled simulations. Next, we extended the CAM5/CLM4-only simulations for an additional 50 years with time varying sea-surface conditions from the final 50 years of the fully coupled simulations. All analyses presented here are based on the final 45 years of the simulations (the first 5 years are discarded as model spin up). We average 45 years of $\delta^{18}O_{\rm p}$ values at each time-slice and compare this value to that of the $\delta^{18}O_{fi}$ values obtained from stalagmite ML-1.

To evaluate the correspondence between $\delta^{13}C_{cc}$ and $\delta^{18}O_{cc}$ values, we calculated the Pearson's correlation and significance (p-values) using the python module 'pearsonr' from SciPy (Virtanen et al., 2020). Additionally, we evaluated the correspondence between the results of this study and published stalagmite records using wild binary segmentation (for further information see Supp. Mat.) (Fryzlewicz, 2014).

4. Results

4.1. Comparison of inclusion fluid and modern meteoric stable isotopic compositions

The measured $\delta^{18}O_{fi}$ and δ^2H_{fi} values range from -11.0 to -6.3% and -86.7 to -65.0%, respectively (Supp. Table 3; Fig. 2A). Despite the fluid inclusion measurements being analyzed on duplicates and not true replicates, the measured $\delta^{18}O_{fi}$ and δ^2H_{fi} values of all duplicates are near the 1σ uncertainty defined by a y=x line (Supp. Fig. 5). The $\delta^{18}O_{fi}$ and δ^2H_{fi} values are well within the range of $\delta^{18}O_{p}$ and δ^2H_{p} values at the Black Chasm locality in the central Sierra Nevada (Oster et al., 2012) and in Sequoia National Park in the southern Sierra Nevada (McCabe-Glynn et al., 2016) (Fig. 2A). Collectively, the $\delta^{18}O_{fi}$ and δ^2H_{fi} values are on average 1‰ offset from the LMWL (Local Meteoric Water Line), but within the range of measured $\delta^{18}O_{p}$ and δ^2H_{p} values when considering all precipitation data for the region (Fig. 2).

4.2. Temporal variability in inclusion-fluid isotopic compositions

For the period of the LG into HS1a, the measured $\delta^{18}O_{fi}$ values of ML-1 are initially constant at ~9‰, after which values decrease by 2‰ and then rise rapidly to a peak of 8‰ at 15 ka (Fig. 3). A subsequent decrease in $\delta^{18}O_{fi}$ (by 2‰) occurs in the OD followed by a rise (by 4‰) to a second peak in the B/A (13.2 ka). Overall, the $\delta^{18}O_{fi}$ and binned $\delta^{18}O_{cc}$ values exhibit little correlation. The δ^2H_{fi} values exhibit low variability through the LG and HS1 periods with a rise around 10‰ beginning at ~15.5 ka followed by a decrease in the BO and a subsequent increase with some variability to 13 ka.

Calculated $\Delta\delta^{18}$ O values over the range of 7 and 12.3 °C span from 33.8 to 31.9% (Fig. 3) using the Tremaine et al. (2011) and Daeron et al. (2019) calcite-water oxygen isotope fractionation equations. The $\Delta\delta^{18}$ O values calculated using the measured

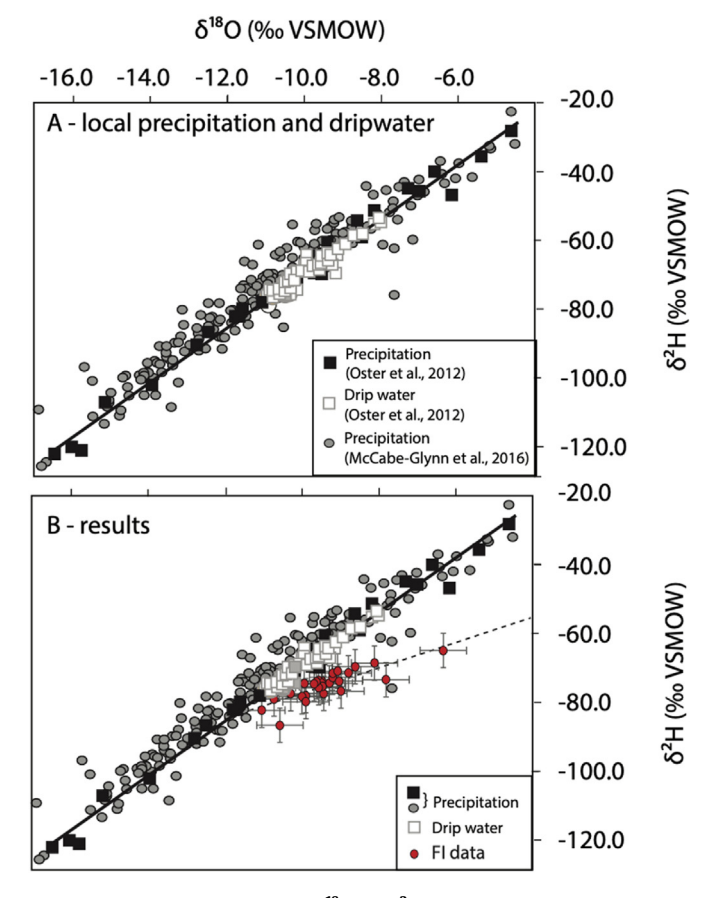


Fig. 2. Precipitation and drip-water $\delta^{18}O$ and δ^2H from CA and comparison to ML-1 $\delta^{18}O_{fi}$ and δ^2H_{fi} values. (A) Local Meteoric Water line (black) defined using Black Chasm (-80 km from McLean's Cave) precipitation data (black squares; Oster et al., 2012). Measured Black Chasm (Oster et al., 2012) drip water (open boxes) and precipitation isotopic compositions (black boxes = Black Chasm, elevation of 680 m; gray circles = Sequoia National Park; elevation of 1921 m (McCabe-Glynn et al., 2016) plot along the local meteoric water line. (B) $\delta^{18}O_{fi}$ and δ^2H_{fi} values for ML-1 (red circles) superimposed on precipitation and drip-water data. Water line based on $\delta^{18}O_{fi}$ and δ^2H_{fi} shown as dashed line. Duplicates are shown in Supp. Fig. 7 ($\delta^2H_{fi}=3.9$ x $\delta^{18}O_{fi}=3.8$ 7). (For interpretation of the references to color in this figure legend, the reader is referred to the Web version of this article.)

inclusion fluid and calcite $\delta^{18}O$ values are lower, ranging between 26 and 32% approaching near equilibrium values between 18 and 15 ka (i.e., through the HS1a and b) and at 14.5 ka (the BO). Calculated d-excess values are overall below that defined by the local meteoric water line (9.8%) and range between -10 and 5%. The *d*-excess values covary with $\delta^{18}O_{fi}$ and 'measured' $\Delta\delta^{18}O$ (Fig. 3). The d-excess values reach minima of -10 and -11% at 15.0 and 13.2 ka. Temperatures calculated using the $\delta^{18}O_{fi}$ and $\delta^{18}O_{cc}$ values (herein referred to as inclusion-fluid-based temperatures) range from 10 to 45 °C (Fig. 4), are mostly higher than modern temperatures measured in Black Chasm (Oster et al., 2012) and are higher than estimated temperatures for the last deglaciation (Tierney et al., 2020). As anticipated, the temperatures exhibit temporal variability that corresponds to changes in $\Delta \delta^{18}$ O and both covary with *d*-excess. Inclusion-fluid temperatures trend to their highest values throughout the LG to early HS1 (19-17.6 ka; 17.4 to 17.2 ka) and through much of the period after 15 ka with peaks at 15.0 and 13.2 ka (Fig. 4), when $\Delta\delta^{18}$ O values are overall low (Fig. 3) and for 15.0 and 13.2 ka, when both $\Delta\delta^{18}$ O and d-excess values reach minimum values. Inclusion-fluid-based temperatures are at their lowest at 17.6 ka, between 17.2 and 15.4 ka (although the data are sparse), and at 14.5 and 13.9 ka (the OD), when $\Delta\delta^{18}$ O values approach predicted equilibrium values and d-excess values are higher. The covariation of all calculated variables indicates that the $\delta^{18}O_{fi}$ and δ^2H_{fi} vary together either through post-entrapment alteration or through in-cave kinetics and evaporation processes.

5. Discussion

To evaluate the preservation of the $\delta^{18}O_{fi}$ and δ^2H_{fi} values for stalagmite ML-1, we applied three tests and conclude that the values are a primary signal and have not been altered postformation. These tests are (i) assessing the stalagmite petrographically for evidence of diagenesis, (ii) evaluating the temperatures at which a change in $\delta^{18}O_{fi}$ and δ^2H_{fi} values would occur, and (iii) comparing the result to the local meteoric water line. We subsequently compare the $\delta^{18}O_{fi}$ and δ^2H_{fi} values with measured $\delta^{18}O_{cc}$ values and the calculated $\Delta\delta^{18}O$ and d-excess values, and the inclusion-fluid-based temperatures. Based on the results presented in the following sections, we hypothesize that the $\delta^{18}O_{fi}$ and $\delta^{2}H_{fi}$ values record shifts in effective moisture through time. Additionally, we discuss how inclusion fluid results can be used to recognize disequilibrium and kinetic fractionation effects and the environmental drivers leading to these effects. We evaluate the inclusionfluid isotopic trends in comparison to published stalagmite and lacustrine proxy records from throughout the Southwest and to earth system model (ESM) simulations of $\delta^{18}O_p$ for the McLean's Cave region. Together these approaches demonstrate that through the interval of the last deglaciation that is recorded in the ML-1 stalagmite (19–13 ka), the $\delta^{18}O_{fi}$ and $\delta^{2}H_{fi}$ time series archive repeated intervals of lower effective moisture in the central Sierra Nevada foothill region, some of which correspond to synchronous periods of inferred lower effective moisture elsewhere in the Southwest.

5.1. Evaluating diagenetic alteration of inclusion fluid stable isotopes

Many early studies have evaluated the utility of measured $\delta^{18}O_{fi}$ values as a robust proxy of drip-water δ^{18} O given the potential for post-formation exchange of oxygen between the stalagmite CaCO₃ and the inclusion fluids (Schwarcz et al., 1976; Harmon et al., 1979; Genty et al., 2001; Demeny et al., 2016). Recent studies, however, have demonstrated that $\delta^{18}O_{fi}$ values are preserved well in the right speleothem material (Van Breukelen et al., 2008; Matthews et al., 2021) Petrographic (transmitted light and epifluorescence; Oster et al., 2015) and coupled X-ray and neutron activation-computed tomographic study (XCT and NCT) of stalagmite ML-1 (Wortham et al., 2019) document banded growth layers free of dissolution features and with systematic distribution of inclusions. The coupled scanning approach also documents the occurrence of inclusions concentrated between elongate crystals indicating their primary origin and the distribution of fluid-filled vs. air-filled inclusions. In this upper 7 cm of the stalagmite, which is characterized by less consistent banding, the fluid-filled inclusions occur as either micropores or macro-pores (Wortham et al., 2019). For the purposes of this study, we have focused on the fluid-filled micro-pores as XCT and NCT scanning as well as petrographic evidence indicate that micro-pores are isolated along growth bands and are not diagenetically altered by post-formation dissolution.

A second test of the primary nature of the inclusion-fluid compositions is to evaluate the possible temperature range that the ML-1 stalagmite may have experienced since formation. Although exposure to temperatures of >105 °C can promote calcite to re-equilibrate in post-formation fluids (Uemura et al., 2020), stalagmite ML-1 has been exposed to a maximum temperature change since formation of $0.0-5.1 \pm 1.7$ °C (Wortham et al., *in*

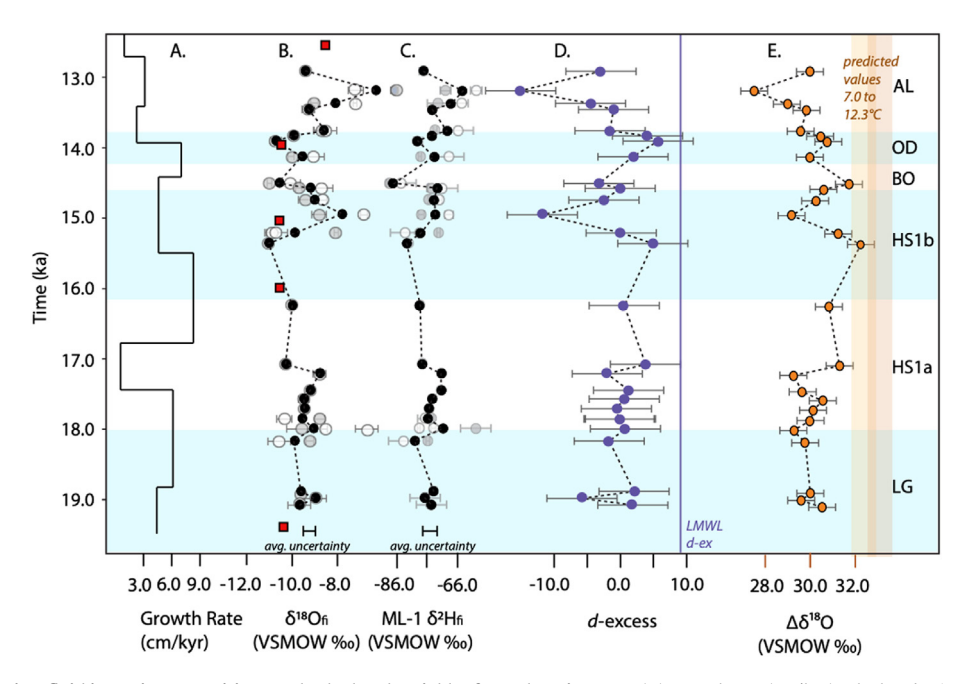


Fig. 3. Time series of inclusion-fluid isotopic compositions and calculated variables for stalagmite ML-1. (A) Growth rate (cm/kyr) calculated using the U-Th-based age model for stalagmite ML-1 (Supp. Fig. 1). (B) δ^{18} O_{fi} and (C) δ^{2} H_{fi} values. Black dots are averaged duplicates. Original measurements with individual uncertainties (see methods) are shown as gray circles. Red squares in (B) represent the average δ^{18} O_p values for 45 years of model results from iCESM1.3 (Tabor et al., 2021; Oster et al., in prep). Note order of magnitude shift between tick marks on A and B. (D) *d*-excess values (purple circles) and comparison to the *d*-excess defined by the LMWL (purple vertical line). (E) $\Delta\delta^{18}$ O values calculated using measured δ^{18} O_{fi} values and the bin-averaged ML-1 δ^{18} O_{cc} values (orange circles) and the range of predicted $\Delta\delta^{18}$ O values (orange vertical bands) defined using bin-averaged ML-1 δ^{18} O_{cc} values, 7.0, 10.0, and 12.3 °C cave temperatures, and the calcite-water oxygen isotope fractionation equations of Tremaine et al. (2011) (light orange) and Daeron et al. (2019) (darker orange). Time increments shown by alternating horizontal blue shading and white intervals. (For interpretation of the references to color in this figure legend, the reader is referred to the Web version of this article.)

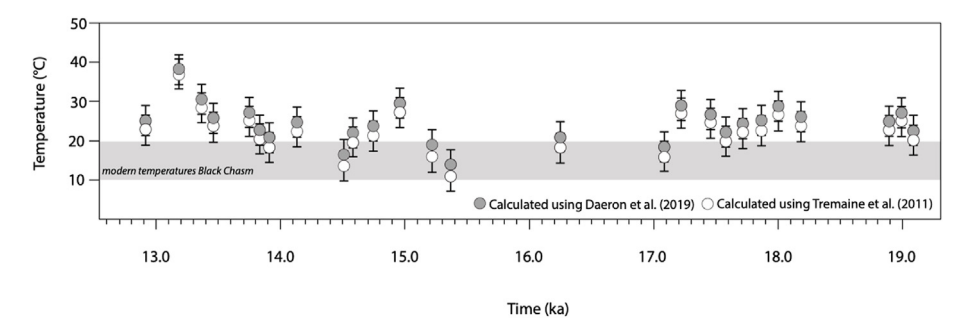


Fig. 4. Temporal trend in inclusion-fluid-based temperatures. Temperatures calculated using the measured $\delta^{18}O_{fi}$ and $\delta^{18}O_{cc}$ values from stalagmite ML-1 and the temperature equations of Tremaine et al. (2011) (open circles) and Daeron et al. (2019) (gray circles). The modern range in temperatures for all drip-sites in Black Chasm (10–20 °C) is shown by the gray bar.

revision) naturally and ~20 °C of temperature change during stalagmite processing and sampling. Additionally, several recent studies (Meckler et al., 2015; Affolter et al., 2015, 2019; Arienzo et al., 2019; Millo et al., 2017; Dassie et al., 2018) have demonstrated that $\delta^{18}O_{fi}$ and $\delta^{2}H_{fi}$ values are well preserved when the inclusion-fluid values generally correspond with the local or global meteoric water lines (Affolter et al., 2015, 2019). As presented in Section 3.1, the $\delta^{18}O_{fi}$ and $\delta^{2}H_{fi}$ values of ML-1 stalagmite generally track the LMWL with an increase to higher δ^{18} O values (up to ~1%) for a given $\delta^2 H$ value for some analyses. These results, however, remain within the range of regional $\delta^{18}O_p$ and δ^2H_p values. On the basis of these three tests, we conclude that the $\delta^{18}O_{fi}$ and δ^2H_{fi} values in the ML-1 stalagmite are a reliable proxy of paleodripwater. The inclusion-fluid values appear to have been moderately modified by evaporative processes in the epikarst or cave prior to their entrapment as inclusions.

5.2. The environmental signal archived in the inclusion-fluid stable isotopic compositions

The $\delta^{18}O_{fi}$ and δ^2H_{fi} values for stalagmite ML-1 indicates variability in the degree of impact of disequilibrium fractionation throughout the record (Fig. 2). Near equilibrium conditions in the cave with minimal evaporation in the region are recorded as the d-excess values falling near the expected value based on the LMWL and for the $\Delta\delta^{18}O$ values falling near the calculated $\Delta\delta^{18}O$ values based on the in-cave temperature equations (Tremaine et al., 2011; Daeron et al., 2019) (Fig. 3). At 14.0 and 15.5 ka, the record indicates that the cave experienced near equilibrium or equilibrium conditions with minimal evaporation in the region. The inclusion-fluid temperatures agree within uncertainty to the temperatures recorded in the Black Chasm (80 km away) during a five-year monitoring effort during these two times (Fig. 4). Finally, the $\delta^{18}O_{fi}$ agree with

the modeled $\delta^{18}O_p$ from iCESM1.3 (Tabor et al., 2021) for the record at these times (Fig. 3). Therefore, stalagmite ML-1 experiences brief periods of equilibrium conditions with minimal evaporation at 14.0 and 15.5 ka.

We interpret variability in d-excess and $\Delta \delta^{18}$ O values away from equilibrium as being driven by disequilibrium in the cave setting driven by lower effective moisture in the region. There are varying degrees of disequilibrium and/or evaporative conditions present in the record, with clear disequilibrium at 15 and 13.2 ka (Fig. 4) where values do not agree with the predictions from the iCESM1.3 output (Tabor et al., 2021). Cave monitoring studies in the Sierra Nevada (Oster et al., 2012; Wortham et al., 2021) demonstrate that relative humidity is variable in Black Chasm (~80 km away; Oster et al., 2012) and that pCO2 is variable at both caves and near atmospheric in the southern Sierra Nevada (Wortham et al., 2021). Based on the modern cave systems, it is possible that disequilibrium isotopic fractionation played a role in driving the $\delta^{18}O_{fi}$ values in the ML-1 stalagmite away from local meteoric water line results. In the modern, low *d*-excess values are associated with evaporative environments (Clark and Fritz, 1997; Lachniet, 2009; Anderson et al., 2016). Low d-excess values have been documented in dripwaters of tropical (Onac et al., 2008; Polk et al., 2012), Mediterranean (Moreno et al., 2014) and semi-arid cave environments (Bar-Matthews and Ayalon, 2004), attributed to seasonal fluctuations in P:E that can lead to 10–30% variability in d-excess values of karst reservoir fluids. Where the evaporation occurred, however, cannot be determined by this variable alone.

The mechanics of calcite-fluid isotopic disequilibrium fractionation in cave environments and the influence on the direction of the resulting change in $\Delta\delta^{18}$ O values (higher or lower) remain debated. For example, cave monitoring studies demonstrate that $\Delta \delta^{18}$ O values increase during periods of disequilibrium fractionation driven by rapid CO2 degassing (independent of relative humidity) that leads to progressive increase in δ^{18} O value of dissolved inorganic carbon (DIC) in the thin-film fluids relative to the bulk drip water and from which the stalagmite calcite precipitates (Mickler et al., 2004; Dreybrodt and Deininger, 2014; Carlson et al., 2020). A model designed to evaluate disequilibrium fractionation during stalagmite formation (Dreybrodt and Deininger, 2014) assumes that the calcite inherits the δ^{18} O value of the DIC from which it precipitates without further modification, leading to increasing $\Delta \delta^{18}$ O value with increasing degree of disequilibrium of calcitefluid isotopic fractionation. Conversely, an ion-by-ion-based model demonstrates that changes in pH and increased growth rate can increase kink mechanisms in calcite growth driving a decrease in $\Delta\delta^{18}O$ values with disequilibrium fractionation (Watkins et al., 2013, 2014). This model of disequilibrium fractionation, however, was developed for fluid-saturated conditions in which $\Delta \delta^{18}$ O value potentially decreases with increasing precipitation rate (Dawans, 1988). *In-situ* studies evaluating disequilibrium fractionation during stalagmite growth have further shown seasonal variability in cave relative humidity and CO₂ degassing can drive $\Delta \delta^{18}$ O values away from predicted values for equilibrium fractionation (e.g., Carlson et al., 2020). The variability in the $\Delta \delta^{18}$ O value is verified by anomalous inclusion-fluid temperatures (Fig. 4) during the same periods. Based on these studies, we suggest that for ML-1 the $\Delta\delta^{18}$ O that fall away from equilibrium are likely driven by kinetic fractionation in the cave.

5.3. Towards a better understanding of $\delta^{18}O_{cc}$ records in the Sierra Nevada using inclusion-fluid stable isotopes

The interpretation of disequilibrium fractionation in the inclusion-fluid record is verified when assessing the covariation between $\delta^{18}O_{cc}$ and $\delta^{13}C_{cc}$ values and by evaluating the trace

element record in stalagmite ML-1. In the past, testing stalagmite records for non-equilibrium fractionation involved assessing whether the $\delta^{13}C_{cc}$ and $\delta^{18}O_{cc}$ values in the stalagmite vary contemporaneously (Meckler et al., 2015; Wong and Breecker, 2015), the "Hendy Test" (Hendy, 1971). Strictly speaking, the Hendy Test evaluates the covariation between $\delta^{18}O_{cc}$ and $\delta^{13}C_{cc}$ along a singl growth layer, however, many researchers use the covariation of $\delta^{18}O_{cc}$ and $\delta^{13}C_{cc}$ through time as a type of Hendy Test for disequilibrium. Covariance in $\delta^{18}O_{cc}$ and $\delta^{13}C_{cc}$ values has been argued to record cave processes such as evaporation or CO₂ ventilation unrelated to climate (e.g., Scroxton et al., 2021). Stalagmite ML-1 reveals covariance between the $\delta^{18}O_{cc}$ and $\delta^{13}C_{cc}$ values, although the slope is low (Oster et al., 2015) (Table 2). Here we further investigate the Hendy Test in stalagmite ML-1 and evaluate the correspondence between $\delta^{18}O_{cc}$ and $\delta^{13}C_{cc}$ values across six-time intervals in the record (Table 2). The correspondence between $\delta^{18}O_{cc}$ and $\delta^{13}C_{cc}$ values is particularly elevated during HS1b (16.1–14.6 ka) and the BO (14.6–14.1 ka) when estimated growth rates are low (Table 2; Fig. 3). The correspondence agrees with the $\Delta \delta^{18}$ O and *d*-excess variability in the inclusion-fluid record. Low growth rate in stalagmite ML-1 is due to less infiltration (lower effective moisture) that leads to a lower ability for the DIC pool in the thin film at the stalagmite site to refresh (Oster et al., 2015). The calcite-based results argue for a higher likelihood of disequilibrium fractionation as seen in the inclusion-fluid results. Some researchers suggest that the Hendy Test is not a reliable test of equilibrium vs. disequilibrium fractionation based on the observation that $\delta^{13}C_{cc}$ values can be influenced by soil properties, respiration, and vegetation variability, all of which can respond to the same climate signals as $\delta^{18}O_{cc}$ (Dorale and Liu, 2009). Therefore, $\delta^{18}O_{cc}$ and $\delta^{13}C_{cc}$ values could covary significantly without being influenced by disequilibrium effects in the cave.

The timing of shifts in the trace element record covary with the inclusion-fluid variability. Trace-element concentrations (Mg, Ba, and Sr) in drip water and calcite precipitated from it have been used to further deconvolve the ambiguity in the Hendy Test because these elements are potentially sensitive to prior calcite precipitation (PCP) and precipitation amount (Fairchild et al., 2000; Wong et al., 2011). The PCP and precipitation amount are directly related to effective moisture and CO₂ degassing, some of the same processes that impact $\delta^{13}C_{cc}$. The trace element time series of stalagmite ML-1 indicate greater prior calcite precipitation (PCP) during HS1 and the AL (Oster et al., 2015), potentially consistent with the hypothesis that Heinrich 1 and the interstadial BO/AL, were drier than the OD stadial. The LG period has a high covariance between $\delta^{18}O_{cc}$ and $\delta^{13}C_{cc},$ suggesting drier conditions, which is consistent with disequilibrium conditions in the LG period in the inclusion-fluid results. The $\delta^{18}O_{cc}$ and $\delta^{13}C_{cc}$ values correlate during periods when the $\Delta\delta^{18}O$ and d-excess decrease away from expected values if the stalagmite precipitated in equilibrium (Fig. 3). We interpret the lower growth rates, lower *d*-excess and $\Delta\delta^{18}$ O, and covariance between δ^{18} O_{cc} and δ^{13} C_{cc} values in certain intervals as recording periods of significantly decreased effective moisture.

5.4. Comparison to published contemporaneous $\delta^{18}O_{cc}$ and δ^2H records

The observed long-term variability in ML-1 $\delta^{18}O_{fi}$ values is broadly similar to the $\delta^{18}O_{cc}$ values measured in a stalagmite from Cave of the Bells (COB; Wagner et al., 2010), and to a lesser extent the time-series of $\delta^{18}O_{cc}$ values in a stalagmite from Fort Stanton, NM (Fig. 5). Moreover, a change-point test for the ML-1 $\delta^{18}O_{fi}$ and COB $\delta^{18}O_{cc}$ values indicates a pronounced shift to higher values at ~15.1 ka in both records (Supp. Fig. 6). The correspondence indicates a regional process impacting the COB and ML-1 records.

With regard to regional $\delta^2 H$ values, the ML-1 $\delta^2 H_{fi}$ exhibits an increase to more positive values between 14 and 15 ka that coincides with the first of a two-step increase in leaf wax $\delta^2 H$ values from Lake Elsinore, CA (Kirby et al., 2013; Feakins et al., 2019) (Fig. 5 and Supp. Fig. 6). A change point calculated for the ML-1 $\delta^2 H_{fi}$ values confirms the statistical significance of this visual comparison (Supp. Fig. 6), suggesting that a common regional driver impacted the Lake Elsinore and ML-1 records on a millennial scale and led to a major shift in regional hydroclimate between 15 and 14 ka.

5.5. Drier times in the Sierra Nevada

We interpret the collective results of this study to indicate temporal variability in regional effective moisture through the late glacial and last deglaciation. This variability includes periods decreased effective moisture (most prominently 15.0 and 13.2 ka) followed by periods of increased effective moisture. To evaluate whether the stalagmite, ML-1, is recording a regional trend we discuss independent evidence of effective moisture. Evidence, independent of stalagmite records, for intervals of decreased effective moisture during the last deglaciation in the US Southwest exists in several lake-level reconstructions (Lake Bonneville, Oviatt et al., 1999; Lake Chewaucan, Cohen et al., 2000; Lake Franklin, Munroe and Laabs, 2013; Lakes Jakes, Clover, and Waring, Garcia and Stokes, 2006; Lake Lahontan, Adams and Wesnousky, 1998; Lake Panamint, Smith, 2009; Lake Russell, Benson et al., 2003; Lake Surprise, Ibarra et al., 2014; comparisons presented in Reheis et al., 2014). Furthermore, a regional compilation of lake highstands documents a southeast to northwest migration of the sites of highest lake levels in the US Southwest through the last deglaciation (McGee et al., 2018). This comparison further documents a rapid shift to decreased moisture delivery to the southern and central part of the Southwest between 16 and 15 ka (McGee et al., 2018), overlapping with the inferred major shift in regional hydroclimate archived in the stalagmite records, including the shift in ML-1 at 15 ka. Shifts in moisture are also captured in transient climate simulations that indicate a reduced moisture budget in the coastal southwestern US (precipitation – evaporation (mm/d)) after 15 ka (Lora and Ibarra, 2019). Collectively, these studies all archive an inferred marked and regional decrease in effective moisture. The combination of the proxies discussed above demonstrates that drying in the central Sierra Nevada did not occur at one step-change, unlike in many other stalagmite and lake records across the Southwest (i.e., McGee et al., 2018) (Supp. Fig. 6). Instead decreases in effective moisture in the central Sierra Nevada occurred in intermittent phases with periods of increased effective moisture interspersed. The difference between the regional trend in the Southwest and the record in stalagmite ML-1 may be due to the Sierra Nevada, which acts as a rain shadow in the modern climate of the Southwest (Crowley et al., 2008). The impact of topography on the regional drying in the Southwest future is a target for future ESM modeling, for studies that utilize high spatial resolution approaches.

6. Summary

We demonstrate the preservation of primary drip-water values, albeit evaporatively enriched in the soil, epikarst, or cave environment, in stalagmite ML-1, through petrographic and scanning analyses and by assessing a range of temperatures at which stalagmite ML-1 would be altered. The inclusion-fluid (δ^{18} O and δ^{2} H) and calcite (δ^{18} O) isotopic records of a stalagmite (ML-1) from a central Sierra Nevada foothill cave (McLean's) and calculated environmentally sensitive values ($\Delta\delta^{18}$ O, d-excess, and inclusionfluid temperature) document repeated periods of disequilibrium oxygen isotopic fractionation in McLean's Cave driven by decreased effective moisture. The timing of decreased effective moisture, in one period from the ML-1 record, is contemporaneous with observed shifts in cave $\delta^{18}\text{O}_{cc}$ values, decreased reconstructed lake levels, and decreased lake δ^2H values from sites of comparable latitude range in the Southwest. The ML-1 record, however, demonstrates many periods of decreased effective moisture and overall

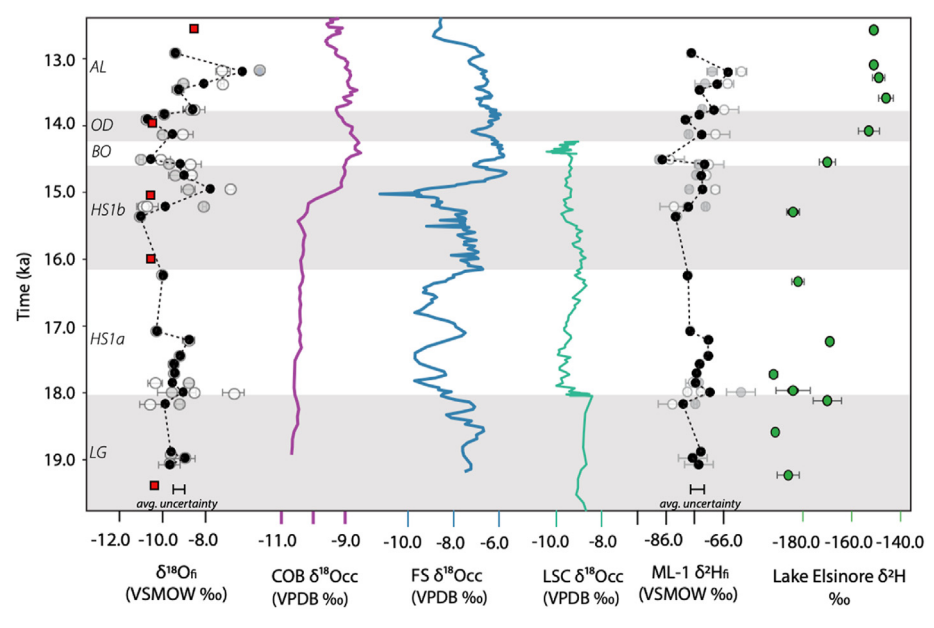


Fig. 5. Time-series of $\delta^{18}O_{fiM}$ and δ^2H_{fi} values in the ML-1 stalagmite compared to published contemporaneous records. (Left) ML-1 $\delta^{18}O_{fi}$ values; black circles represent the time series, and the gray circles are the duplicate measurements. To the immediate right, $\delta^{18}O_{cc}$ time series for three southwestern stalagmites: purple — Cave of the Bells (COB; Wagner et al., 2010); blue — Fort Stanton (FS; Asmerom et al., 2010); green — Lake Shasta Cave (LSC; Oster et al., 2020). Second from the right: inclusion-fluid δ^2H time-series for ML-1 (symbols as in the $\delta^{18}O_{fi}$ time series) and Lake Elsinore lead-wax δ^2H record (green circles; Kirby et al., 2013; Feakins et al., 2019). Time intervals are noted as alternating horizontal gray shading and white intervals. Uncertainty on isotopic measurements is indicated by capped horizontal lines. (For interpretation of the references to color in this figure legend, the reader is referred to the Web version of this article.)

greater variability than regional stalagmite and lake records from the east side of the Sierra Nevada. The comparison suggests that McLean's cave and the western side of the Sierra Nevada may be more sensitive to changes in effective moisture. This study allows for a greater understanding of how stalagmite records in the Southwest document and record effective moisture.

Declaration of competing interest

The authors declare that they have no known competing financial interests or personal relationships that could have appeared to influence the work reported in this paper.

Acknowledgements

This work was supported by NSF grants AGS-1420079 and AGS-1444210 to IPM, AGS-1805213 to PKS, and AGS-1804747 to CT., and the Durrell Grant and Ernest E. Hill Fellowship awarded to BEW. We thank Dave Hodell for suggesting the use of the platinum catalyst.

Appendix A. Supplementary data

Supplementary data to this article can be found online at https://doi.org/10.1016/j.quascirev.2022.107399.

References

- Adams, K.D., Wesnousky, S.G., 1998. Shoreline processes and the age of the Lake Lahontan highstand in the Jessup embayment, Nevada. Geol. Soc. Am. Bull. 110 (10), 1318–1332. https://doi.org/10.1130/0016-7606(1998)110<1318: SPATAO>2.3.CO:2.
- Affolter, S., Hauselmann, A.D., Fleitmann, D., Hauselmann, P., Leuenberger, M., 2015. Triple isotope (δD, δ¹⁷O, δ¹⁸O) study on precipitation, drip-water and speleothem fluid inclusions for a Western Central European cave (NW Switzerland). Ouat. Sci. Rev. 127, 73–89. https://doi.org/10.1016/j.quascirev.2015.08.030.
- Affolter, S., Hauselmann, A., Fleitmann, D., Edwards, R.L., Cheng, H., Leuenberger, M., 2019. Central Europe temperature constrained by speleothem fluid inclusion water isotopes over the past 14000 years. Sci. Adv. 5 (6), eaav3809. https://doi.org/10.1126/sciadv.aav3809.
- Allen, B.D., Anderson, R.Y., 2000. A continuous, high-resolution record of late Pleistocene climate variability from the Estancia basin, New Mexico. GSA Bulletin 112 (9), 1444–1458. https://doi.org/10.1130/0016-7606(2000) 112-1444:ACHRRO>2.0.CO:2.
- Anderson, L., Berkelhammer, M., Mast, M.A., 2016. Isotopes in north American rocky mountain snowpack 1993-2014. Quat. Sci. Rev. 131 (B), 262–273. https://doi.org/10.1016/j.quascirev.2015.03.023.
- Asmerom, Y., Polyak, V.J., Burns, S.J., 2010. Variable winter moisture in the south-western United States linked to rapid glacial climate shifts. Nat. Geosci. 3, 114–117. https://doi.org/10.1038/ngeo754.
- Asmerom, Y., Polyak, V.J., Lachniet, M.S., 2017. Extrapolar climate reversal during the last deglaciation. Sci. Rep. 7, 7157. https://doi.org/10.1038/s41598-017-07721-8.
- Ayalon, A., Bar-Matthews, M., Frumkin, A., Matthews, A., 2013. Last Glacial warm events on Mount Hermon: the southern extension of the Alpine karst range of the east Mediterranean. Ouat. Sci. Rev. 59, 43–56.
- Arienzo, M.M., Swart, P.K., Vonhof, H.B., 2013. Measurement of d180 and d2H values of fluid inclusion water in speleothems using cavity ring-down spectroscopy compared with isotope ratio mass spectrometry. Rapid Commun. Mass Spectrom. 27, 2616–2624. https://doi.org/10.1002/rcm.6723.
- Arienzo, M.M., Swart, P.K., Pourmand, A., Broad, K., Clement, A.C., Murphy, L.N., Vonhof, H.B., Kakuk, B., 2015. Bahamian speleothem reveals temperature decrease associated with Heinrich stadials. Earth Planet Sci. Lett. 430, 377–386. https://doi.org/10.1016/j.epsl.2015.08.035.
- Arienzo, M.M., Mehterian, S., Swart, P.K., Broad, K., Kakuk, B., 2019. Drip-water and calcite geochemistry variations in a monitored Bahamas cave. G-cubed 20, 1–13. https://doi.org/10.1029/2019GC008339.
- Banner, J.L., Guilfoyle, A., James, E.W., Stern, L.A., Musgrove, M., 2007. Seasonal variations in modern speleothem calcite growth in central Texas, U.S.A. J. Sediment. Res. 77 (8), 615–622. https://doi.org/10.2110/jsr.2007.065.
- Bar-Matthews, M., Ayalon, A., 2004. Speleothems as palaeoclimate indicators, a case study from Soreq Cave located in the Eastern Mediterranean Region, Israel. In: Battarbee, R.W., Gasse, F., Stickley, C.E. (Eds.), Past Climate Variability through Europe and Africa. Developments in Paleoenvironmental Research, vol. 6. Springer, Dordrecht. https://doi.org/10.1007/978-1-4020-2121-3_18.
- Benson, L., Lund, S., Negrini, R., Linsley, B., Zic, M., 2003. Response of North American Great Basin lakes to Dansgaard-Oeschger oscillations. Quat. Sci. Rev. 22 (21–22), 2239–2251. https://doi.org/10.1016/S0277-3791(02)00249-4.

- Bacon, S.N., Burke, R.M., Pezzopane, S.K., Jayko, A.S., 2006. Last glacial maximum and Holocene lake levels of Owens Lake, eastern California, USA. Qua. Sci. Res. 25 (11–12), 1264–1282. https://doi.org/10.1016/j.quascirev.2005.10.014.
- Brietenbach, S.F.M., Rehfeld, K., Goswami, B., Baldini, J.U.L., Ridley, H.E., Kennett, D.J., Prufer, K.M., Aquino, V.V., Asmerom, Y., Polyak, V.J., Cheng, H., Kurths, J., Marwan, N., 2012. Constructing Proxy Records from Age models (COPRA). Clim. Past 8, 1765–1779. https://doi.org/10.5194/cp-8-1765-2012.
- Broecker, W., Putnam, A.E., 2013. Hydrologic impacts of past shifts of Earth's thermal equator offer insight into those to be produced by fossil fuel CO₂. Proc. Natl. Acad. Sci. U.S.A. 110, 16710–16715. https://doi.org/10.1073/pnas.1301855110.
- Broecker, W.S., McGee, D., Adams, K.D., Cheng, H., Edwards, R.L., Oviatt, C.G., Quade, J., 2009. A Great Basin-wide dry episode during the first half of the Mystery Interval? Quat. Sci. Rev. 28 (25–26), 2557–2563. https://doi.org/10.1016/j.quascirev.2009.07.007.
- Carlson, P.E., Noronha, A.L., Banner, J.L., Jenson, J.W., Moore, M.W., Partin, J.W., Deininger, M., Breecker, D.O., Bautista, K.K., 2020. Geochem. Cosmochim. Acta 284, 222–238. https://doi.org/10.1016/j.gca.2020.06.012.
- Clark, I.D., Fritz, P., 1997. Environmental Isotopes in Hydrogeology, first ed. CRC Press. https://doi.org/10.1201/9781482242911.
- Cohen, A., Palacios-Fest, M., Negrini, R., Wigand, P., Erbes, D., 2000. A paleoclimate record for the past 250,000 years from Summer Lake, Oregon, USA: II. Sedimentology, paleontology and geochemistry. J. Paleolimnol. 24 (2), 151–182. https://doi.org/10.1023/A:1008165326401.
- Crowley, B.E., Koch, P.L., Davis, E.B., 2008. Stable isotope constraints on the elevation history of the Sierra Nevada Mountains, California. Geol. Soc. Am. Bull. 120 (5–6), 588–598. https://doi.org/10.1130/B26254.1.
- Daeron, M., Drysdale, R.N., Peral, M., Huyghe, D., Blamart, D., Coplen, T.B., Lartaud, F., Zanchetta, G., 2019. Most Earth-surface calcites precipitate out of isotopic equilibrium. Nature Comms 10, 429. https://doi.org/10.1038/s41467-019-08336-5.
- Dassie, E.P., Genty, D., Noret, A., Mengenot, X., Massault, M., Lebas, N., Duhamel, M., Bonifacie, M., Gasparrini, M., Minster, B., Michelot, J.-L., 2018. A newly designed analytical line to examine fluid inclusion isotopic compositions in a variety of carbonate samples. G-cubed 19 (4), 1107–1122. https://doi.org/10.1002/ 2017GC007289.
- Dawans, J.M., 1988. Textural and geochemical alternations in late Cenozoic Bahamian dolomites. Sedimentology 35, 385–403. https://doi.org/10.1111/j.1365-30911988 tb00993 x
- De Graaf, S., Vonhof, H.B., Weissbach, T., Wassenburg, J.A., Levy, E.J., Kluge, T., Haug, G.H., 2020. A comparison of isotope ratio mass spectrometry and cavity ring-down spectroscopy techniques for isotope analysis of fluid inclusion water. Rapid Commun. Mass Spectrometry 34 (16), e8837. https://doi.org/10.1002/rcm.8837.
- De Wet, C.B., Erhardt, A.M., Sharp, W.D., Marks, N.E., Bradbury, H.J., Turchyn, A.V., Xu, Y., Oster, J., 2021. Semiquantitative estimates of rainfall variability during the 8.2 kyr event in California using speleothem calcium isotope ratios. Geophys. Res. Lett. 48 (3), e2020GL089154. https://doi.org/10.1029/2020GL089154.
- Demeny, A., Czuppon, G., Kern, Z., Leel-Ossy, S., Nemeth, A., Szabo, M., Toth, M., Wu, C.-C., Shen, C.-C., Molnar, M., Nemeth, T., Nemeth, P., Ovari, M., 2016. Recrystallization-induced oxygen isotope changes in inclusion-hosted water of speleothems- Paleoclimatological implications. Quat. Int. 415, 25–32. https://doi.org/10.1016/j.quaint.2015.11.137.
- Dorale, J.A., Liu, Z., 2009. Limitations of Hendy test criteria in judging the paleoclimatic suitability of speleothems and the need for replication. J. Cave Karst Stud. 71 (1), 73–80.
- Dreybrodt, W., Deininger, M., 2014. The impact of evaporation to the isotope composition of DIC in calcite precipitating water films in equilibrium and kinetic fractionation models. *Geochem. Cosmochim. Acta* 125, 433–439. https://doi.org/10.1016/j.gca.2013.10.004.
- Fairchild, I.J., Borsato, A., Tooth, A.F., Frisia, S., Hawkesworth, C.J., Huang, Y., McDermott, F., Sprio, B., 2000. Controls on trace element (Sr-Mg) compositions of carbonate cave waters: implications for speleothem climatic records. Chem. Geol. 166, 255–269. https://doi.org/10.1016/S0009-2541(99)00216-8.
- Feakins, S.J., Wu, M.S., Ponton, C., Tierney, J.E., 2019. Biomarkers reveal abrupt switches in hydroclimate during the last glacial in southern California. Earth Planet Sci. Lett. 515, 164–172. https://doi.org/10.1016/j.epsl.2019.03.024.
- Forbes, J., 1998. Air temperature and relative humidity study: Torgac Cave, New Mexico. J. Cave Karst Stud. 60 (1), 27–32.
- Fryzlewicz, P., 2014. Wild binary segmentation for multiple change-point detection. Ann. Stat. 42 (6), 2243–2281. https://doi.org/10.1214/14-AOS1245.
- Garcia, A.F., Stokes, M., 2006. Late Pleistocene highstand and recession of a small, high-altitude, pluvial lake, Jakes Valley, central Great Basin, USA. Quat. Res. 65, 179–186. https://doi.org/10.1016/j.yqres.2005.08.025.
- Genty, D., Baker, A., Vokal, B., 2001. Intra- and inter-annual growth rate of modern stalagmites. Chem. Geol. 176, 191–212. https://doi.org/10.1016/S0009-2541(00)
- Griffiths, M.L., Drysdale, R.N., Vonhof, H.B., Gagan, M.K., Zhao, J.-x., Ayliffe, L.K., Hantoro, W.S., Hellstrom, J.C., Cartwright, I., Frisia, S., Suwargadi, B.W., 2010. Younger Dryas-Holocene temperature and rainfall history of southern Indonesia from d180 in speleothem calcite and fluid inclusions. Earth Planet Sci. Lett. 295, 30–36. https://doi.org/10.1016/j.epsl.2010.03.018.
- Harmon, R.S., Schwarcz, H.P., O'Neil, J.R., 1979. D/H ratios in speleothem fluid inclusions: A guide to variations in the isotopic composition of meteoric precipitation? Earth Planet Sci. Lett. 42, 254–266. https://doi.org/10.1016/0012-821X(79)90033-5.

- He, C., Liu, Z., Otto-Bliesner, B.L., Brady, E.C., Zhu, C., Tomas, R., et al., 2021. Hydroclimate footprint of pan-Asian monsoon water isotope during the last deglaciation. Sci. Adv. 7 (4), eabe2611.
- Hendy, C.H., 1971. The isotopic geochemistry of speleothems-I. The calculation of the effects of different modes of formation on the isotopic composition of speleothem and their applicability as paleoclimatic indicators. Geochem. Cosmochim. Acta 35 (8), 801–824. https://doi.org/10.1016/0016-7037(71)90127-X.
- Hudson, A.M., Hatchett, B.J., Quade, J., Boyle, D.P., Bassett, S.D., Ali, G., Marie, G., 2019. North-south dipole in winter hydroclimate in the western United States during the last deglaciation. Sci. Rep. 9 (1), 1–12. https://doi.org/10.1038/s41598-019-41197-v.
- Ibarra, D.E., Egger, A.E., Weaver, K.L., Harris, C.R., Maher, K., 2014. Rise and fall of late Pleistocene pluvial lakes in response to reduced evaporation and precipitation: Evidence from Lake Surprise, California. Bulletin 126 (11–12), 1387–1415. https://doi.org/10.1130/B31014.1.
- Kirby, M.E., Feakins, S.J., Bonuso, N., Fantozzi, J.M., Hiner, C.A., 2013. Latest Pleistocene to Holocene hydroclimates from Lake Elsinore, California. Quat. Sci. Rev. 76, 1–15. https://doi.org/10.1016/j.quascirev.2013.05.023.
- Lachniet, M.S., 2009. Climatic and environmental controls on speleothem oxygenisotope values. Quat. Sci. Rev. 28, 412–432. https://doi.org/10.1016/ j.quascirev.2008.10.021.
- Lachniet, M.S., Denniston, R.F., Asmerom, Y., Polyak, V.J., 2014. Orbital control of western North America atmospheric circulation and climate over two glacial cycles. Nat. Commun. 5, 3805. https://doi.org/10.1016/j.quascirev.2008.10.021.
- Lachniet, M.S., 2016. A speleothem record of Great Basin paleoclimate: The Leviathan chronology, Nevada, Chapter 20. In: Shroder Jr., J.F. (Ed.), Lake Bonneville: A Scientific Update, *Developments in Earth Surface Processes*, vol. 20, pp. 551–569.
- Lora, J.M., Ibarra, D.E., 2019. The North American hydrologic cycle through the last deglaciation. Quat. Sci. Rev. 226, 105991. https://doi.org/10.1016/ j.quascirev.2019.105991.
- Matthews, A., Affek, H.P., Ayalon, A., Vonhof, H.B., Bar-Matthews, M., 2021. Eastern Mediterranean climate change deduced from Soreq Cave fluid inclusion stable isotopes and carbonate clumped isotopes record of the last 160 ka. Quat. Sci. Rev. 272. 107223.
- McCabe-Glynn, S., Johnson, K., Strong, C., Zou, Y., Yu, J.-Y., Sellars, S., Welker, J.M., 2016. Isotopic signature of extreme precipitation events in the western U.S. and associated phases of Arctic and tropical climate modes. J. Geophys. Res. Atmos. 121 (15), 8913–8924. https://doi.org/10.1002/2016JD025524.
- McDermott, F., 2004. Palaeo-climate reconstruction from stable isotope variations in speleothems: a review. Quat. Sci. Rev. 23 (7–8), 908–918. https://doi.org/ 10.1016/j.quascirev.2003.06.021.
- McGarry, S., Bar-Matthews, M., Matthews, A., Vaks, A., Schilman, B., Ayalon, A., 2004. Constraints on hydrological and paleotemperature variations in the Eastern Mediterannean region in the last 140 ka given by the dD values of speleothem fluid inclusions. Quat. Sci. Rev. 23 (7–8), 919–934. https://doi.org/10.1016/j.quascirev.2003.06.020.
- McGee, D., Quade, J., Edwards, R.L., Broecker, W.S., Cheng, H., Reiners, P.W., Evenson, N., 2012. Lacustrine cave carbonates: novel archives of paleohydrologic change in the Bonneville Basin (Utah, USA). Earth Planet Sci. Lett. 351–352, 182–194. https://doi.org/10.1016/j.epsl.2012.07.019.
- McGee, D., Moerno-Chamarro, E., Marshall, J., Galbraith, E.D., 2018. Western U.S. lake expansions during Heinrich stadials linked to Pacific Hadley circulation. Sci. Adv. 4 (11), eaav0118. https://doi.org/10.1126/sciadv.aav0118.
- Meckler, A.N., Affolter, S., Dublyansky, Y.V., Kruger, Y., Vogel, N., Bernasconi, S.M., Frenz, M., Kipfer, R., Leuenberger, M., Spotl, C., 2015. Glacial-interglacial temperature change in the tropical West Pacific: a comparison of stalagmite-based paleo-thermometers. Quat. Sci. Rev. 127, 90–116. https://doi.org/10.1016/j.quascirev.2015.06.015.
- Mickler, P.J., Banner, J.L., Stern, L., Asmerom, Y., Edwards, R.L., Ito, E., 2004. Stable isotope variations in modern tropical speleothem: evaluating equilibrium vs. kinetic isotope effects. Geochem. Cosmochim. Acta 68, 4381–4393. https://doi.org/10.1016/j.gca.2004.02.012.
- Mickler, P.J., Stern, L.A., Banner, J.L., 2006. Large kinetic isotope effects in modern speleothems. GSA Bulletin 118 (1–2), 65–81. https://doi.org/10.1130/B25698.1.
- Millo, C., Strikis, N.M., Vonhof, H.B., Deininger, M., Cruz, F.W., Wang, X., Cheng, H., Edwards, R.L., 2017. Last glacial and Holocene stable isotope record of fossil drip-water from subtropical Brazil based on analysis of fluid inclusions in stalagmites. Chem. Geol. 468, 84–96. https://doi.org/10.1016/ j.chemgeo.2017.08.018.
- Moreno, A., Sancho, C., Barolome, M., Oliva-Urcia, B., Delgado-Huertas, A., Estrela, M.J., Corell, D., Lopez-Moreno, J.I., Cacho, I., 2014. Climate controls on rainfall isotopes and their effects on cave drip-water and speleothem growth: the case of Molinos cave (Teruel, NE Spain). Clim. Dynam. 43, 221–241. https://doi.org/10.1007/s00382-014-2140-6.
- Munroe, J.S., Laabs, B.J.C., 2013. Temporal correspondence between pluvial lake highstands in the southwestern US and Heinrich Event 1. J. Quat. Sci. 28 (1), 49–58. https://doi.org/10.1002/jqs.2586.
- Onac, B.P., Pace- Graczyk, K., Atudirei, V., 2008. Stable isotope study of precipitation and cave drip-water in Florida (USA): implications for speleothem based paleoclimate studies. Isot. Environ. Health Stud. 44 (2), 149–161. https://doi.org/10.1080/10256010802066174.
- Oster, J.L., Montanez, I.P., Sharp, W.D., Cooper, K.M., 2009. Late Pleistocene California droughts during deglaciation and Arctic warming. Earth Planet Sci. Lett. 288 (3–4), 434–443. https://doi.org/10.1016/j.epsl.2009.10.003.

- Oster, J.L., Montanez, I.P., Kelley, N.P., 2012. Response of a modern cave system to large seasonal precipitation variability. Geochem. Cosmochim. Acta 91, 92–108. https://doi.org/10.1016/j.gca.2012.05.027.
- Oster, J.L., Montanez, I.P., Santare, L.R., Sharp, W.D., Wong, C., Cooper, K.M., 2015. Stalagmite records of hydroclimate in central California during termination 1. Quat. Sci. Rev. 127, 199—214. https://doi.org/10.1016/j.quascirev.2015.07.027.
- Oster, J.L., Weisman, I.E., Sharp, W.D., 2020. Multi-proxy stalagmite records from northern California reveal dynamic patterns of regional hydroclimate over the last glacial cycle. Quat. Sci. Rev. 241, 106411. https://doi.org/10.1016/j.quascirev.2020.106411.
- Oviatt, C.G., Thompson, R.S., Kaufman, D.S., Bright, J., Forester, R.M., 1999. Reinter-pretation of the Burmester core, Bonneville basin, Utah. Quat. Res. 52 (2), 180–184. https://doi.org/10.1006/qres.1999.2058.
- Owen, L.A., Finkel, R.C., Minnich, R.A., Perez, A.E., 2003. Extreme southwestern margin of late Quaternary glaciation in North America: timing and controls. Geology 31 (8), 729–732. https://doi.org/10.1130/G19561.1.
- Polk, J.S., van Beynen, P., Wynn, J., 2012. An isotopic calibration study of precipitation, cave drip-water, and climate in west-central Florida. Hydrol. Process. 26 (5), 652–662. https://doi.org/10.1002/hyp.8169.
- Quade, J., Broecker, W.S., 2009. Dryland hydrology in a warmer world: Lessons from the Last Glacial period. Eur. Phys. J. Spec. Top. 176 (1), 21–36. https://doi.org/ 10.1140/epjst/e2009-01146-y.
- Reheis, M.C., Adams, K.D., Oviatt, C.G., Bacon, S.N., 2014. Pluvial lakes in the Great Basin of the western United States—A view from the outcrop. Quat. Sci. Rev. 97, 33–57. https://doi.org/10.1016/j.quascirev.2014.04.012.
- Rogerson, M., Dublyansky, Y., Hoffmann, D.L., Luetscher, M., Tochterle, P., Spotl, C., 2019. Enhanced Mediterranean water cycle explains increased humidity during MIS 3 in North Africa. Clim. Past 15, 1757–1769. https://doi.org/10.5194/cp-15-1757-2019.
- Rozanski, K., Araguas-Araguas, L., Gonfiantini, R., 1993. Isotopic patterns in modern global precipitation. Climate change in continental isotopic records. Geophys. Monogr. 78, 1–1.
- Santare, L.R., 2013. A Multi-Proxy Stalagmite Reconstruction of Climate in the Central Sierra Nevada during the Last Deglaciation. University of California, Davis Thesis, p. 1548292.
- Santi, L.M., Arnold, A.J., Ibarra, D.E., Whicker, C.A., Mering, J.A., Lomarda, R.B., Lora, J.M., Tripati, A., 2020. Clumped isotope constraints on changes in latest Pleistocene hydroclimate in the northwestern Great Basin: Lake Surprise, California. GSA Bulletin 132 (11–12), 2669–2683. https://doi.org/10.1130/B35484.1.
- Schwarcz, H.P., Harmon, R.S., Thompson, P., Ford, D.C., 1976. Stable isotope studies of fluid inclusions in speleothems and their paleoclimate significance. Geochem. Cosmochim. Acta 40 (6), 657–665. https://doi.org/10.1016/0016-7037(76) 90111-3.
- Scroxton, N., Walczak, M., Markowska, M., Zhao, J.X., Fallon, S., 2021. Historical droughts in Southeast Australia recorded in a New South Wales stalagmite. Holocene 31 (4), 607–617. https://doi.org/10.1177/0959683620981717.
- Smith, G.I., 2009. Late Cenozoic geology and lacustrine history of Searles Valley, Inyo and San Bernardino Counties. In: US Geological Survey, California, p. 115.
- Street, J.H., Anderson, R.S., Paytan, A., 2012. An organic geochemical record of Sierra Nevada climate since the LGM from Swamp Lake, Yosemite. Quat. Sci. Rev. 40, 89–106. https://doi.org/10.1016/j.quascirev.2012.02.017.
- Tabor, C., Lofverstrom, M., Oster, J., Wortham, B.E., de Wet, C., Montanez, I., Rhoades, A., Zarzycki, C., He, C., Liu, Z., 2021. A mechanistic understanding of oxygen isotopic changes in the western United States at the Last Glacial Maximum. Quat. Sci. Rev. 274, 107255. https://doi.org/10.1016/ j.quascirev.2021.107255.
- Tierney, J.E., Zhu, J., King, J., Malevich, S.B., Hakim, G.J., Poulsen, C.J., 2020. Glacial cooling and climate sensitivity revisited. Nature 584, 569–573. https://doi.org/10.1038/s41586-020-2617-x.
- Tremaine, D.M., Froelich, P.N., Wang, Y., 2011. Speleothem calcite farmed *in situ*: modern calibration of δ^{18} O and δ^{13} C paleoclimate proxies in a continuously-monitored natural cave system. Geochem. Cosmochim. Acta 75 (17), 4929–4950. https://doi.org/10.1016/j.gca.2011.06.005.
- Uemura, R., Kina, Y., Shen, C.-C., Omine, K., 2020. Experimental evaluation of oxygen isotopic exchange between inclusion water and host calcite in speleothems. Clim. Past 16, 17–27. https://doi.org/10.5194/cp-16-17-2020.
- Van Breukelen, M.R., Vonhof, H.B., Hellstrom, J.C., Wester, W.C.G., Kroon, D., 2008. Fossil dripwater in stalagmites reveals Holocene temperature and rainfall variation in Amazonia. Earth Planet Sci. Lett. 275, 54–60.
- Virtanen, P., Gommers, R., Oliphant, T.E., Haberland, M., Reddy, T., Cournapeau, D., Van Mulbregt, P., 2020. SciPy 1.0: fundamental algorithms for scientific computing in Python. Nat. Methods 17 (3), 261–272. https://doi.org/10.1038/ s41502-019-0686-2
- Vonhof, H.B., van Breukelen, M.R., Pstma, O., Rowe, P.J., Atkinson, T.C., Kroon, D., 2006. A continuous-flow crushing device for on-line d2H analysis of fluid inclusion water in speleothems. Rapid Commun. Mass Spectrom. 20 (17), 2553–2558. https://doi.org/10.1002/rcm.2618.
- Wagner, J.D.M., Cole, J.E., Beck, J.W., Patchett, P.J., Henderson, G.M., Barnet, H.R., 2010. Moisture variability in the southwestern United States linked to abrupt glacial climate change. Nat. Geosci. 3, 110–113. https://doi.org/10.1002/ rcm.2618.
- Watkins, J.M., Nielsen, L.C., Ryerson, F.J., DePaolo, D.J., 2013. The influence of kinetics on the oxygen isotope composition of calcium carbonate. Earth Planet Sci. Lett. 375, 349–360. https://doi.org/10.1016/j.epsl.2013.05.054.
- Watkins, J.M., Hunt, J.D., Ryerson, F.J., DePaulo, D.J., 2014. The influence of

- temperature, pH, and growth rate on the d18O composition of inorganically precipitated calcite. Earth Planet Sci. Lett. 404, 332–343. https://doi.org/10.1016/j.epsl.2014.07.036.
- Warken, S.F., Weissbach, T., Kluge, T., Vonhof, H., Scholz, D., Vieten, R., Schmidt, M., Winter, A., Frank, N., 2021. Last glacial millennial-scale hydro-climate and temperature change in Puerto Rico constrained by speleothem fluid inclusion d18O and d2H values. Clim. Past. https://doi.org/10.1016/j.quascirev.2015.07.019.
- Western Regional Climate Center. Evaporation Stations: California, New Melones Dam. Accessed on Aug. 31, 2019. https://wrcc.dri.edu/Climate/comp_table_show.php?stype=pan_eyap_avg.
- Wong, C.I., Banner, J.L., 2010. Response of cave air CO2 and drip water to brush clearing in central Texas: implications for recharge and soil CO2 dynamics. J. Geophys. Res.: Biogeosciences 115, G04018. https://doi.org/10.1029/2010|G001301.
- Wong, C.I., Banner, J.L., Musgrove, M., 2011. Seasonal drip-water Mg/Ca and Sr/Ca variations driven by cave ventilation: implications for and modeling of

- speleothem paleoclimate records. Geochem. Cosmochim. Acta 75 (12), 3514–3529. https://doi.org/10.1016/j.gca.2011.03.025.
- Wortham, B.E., Montañez, I.P., Rowland, D.J., Lerche, M., Browning, A., 2019. Mapping fluid-filled inclusions in stalagmites using coupled X-ray and neutron computed tomography: Potential as a water excess proxy. G-cubed 20 (6), 2647–2656. https://doi.org/10.1029/2018GC008140.
- Wong, C.I., Breecker, D.O., 2015. Advancements in the use of speleothems as climate archives. Quat. Sci. Rev. 127, 1–18. https://doi.org/10.1016/i.guascirey.2015.07.019.
- Wortham, B.E., Montañez, I.P., Bowman, K.C., Kuta, D.J., Brumage, E., Pang, A., Soto, N., Tinsley, J., Roemer-Baer, G., 2021. Cave monitoring of Sierra Nevada caves reveals the potential for stalagmites to archive seasonal variability. Frontiers in Earth Science, section Quaternary Science, Geomorphology and Paleoenvironment 9, 781526. https://doi.org/10.3389/feart.2021.781526.
- Zheng, L., Ma, J., Sun, X., Guo, X., Cheng, Q., Shi, X., 2018. Estimating the root water uptake of surface-irrigated apples using water stable isotopes and the Hydrus-1D model. Water 10, 1624. https://doi.org/10.3390/w10111624.